Int. J. Heat Mass Transfer. Vol. 36, No. 2, pp. 437–452, 1993
Printed in Great Britain

0017-9310/93 $6.00+0.00

Transient thermal convection in an enclosure induced simultaneously by gravity and vibration

WU-SHUNG FU

Department of Mechanical Engineering, National Chiao Tung University, Hsinchu, Taiwan 300, R.O.C.

and

WEN-JIANN SHIEH

Energy & Resources Labs, Industrial Technology Research Institute, Hsinchu, Taiwan 310, R.O.C.

(*Received* 20 *May* 1991 *and in final form* 3 *February* 1992)

Abstract—Transient thermal convection in a two-dimensional square enclosure induced simultaneously by gravity and vibration is investigated numerically. The enclosure, which is filled with air under a terrestrial environment, is insulated at both horizontal walls and kept at constant temperature at the vertical walls. For time $t = 0$, the fluid is stationary with the same temperature as the vertical walls T_c; as $t > 0$, the left wall temperature is raised to T_h and the enclosure is vibrated with a constant frequency Ω and amplitude b simultaneously. In order to study the effect of vibration frequency on the transient thermal convection, four vibration frequencies (100, 900, 1100, 5000) are considered with fixed Rayleigh number ($Ra = 10^4$) and vibrational Grashof number ($G = 10^6$). The results show that the transient process, from the stationary state to the steady flow state, is shortened by increasing the vibration frequency, and both the flow field and heat transfer mechanism are mainly determined by the vortex shedding rate, which has the same frequency as the vibration frequency near the upper and lower corners of the hot wall. For $\omega = 100$, a single main cell is formed and alternates the rotating direction with the variation of the buoyancy force direction. For $\omega = 5000$, the buoyancy force induced by the vibration is definitely dominant and the development of temperature distribution from left to right sides is initially symmetric at the center line of the vertical wall; afterwards, an instability of the thermal boundary layer causes an overshoot of the total Nusselt number and an increase of flow intensity before the periodic solution is approached. For $\omega = 900$ and 1100, the vortices shed continuously and alternately from the upper and lower corners near the hot wall, which causes the variation of the total Nusselt number to be irregular and inconsistent on the hot and cold walls for the $\omega = 900$ case; for the $\omega = 1100$ case the total Nusselt number varies irregularly in the transient processes, but a periodic solution is obtained at steady state.

INTRODUCTION

NATURAL convection in an enclosure has received a great deal of attention in the past, but studies on the thermal convection in an enclosure induced simultaneously by gravity and vibration, which is important in material processing [1, 2] or in heat transfer under a vibrational environment [3], are very rare. Forbes *et al.* [4] studied experimentally the thermal convection in a vertical rectangular enclosure filled with liquid. They varied the vibration frequency and acceleration to find the effect of vibration on the heat transfer rate. It was shown that the heat transfer rate was increased by the vibration, especially near the resonant natural frequency of the liquid column contained within the enclosure. Ivanova and Kozlov [5] vibrated the fluid layer between the concentric cylinders vertically. Different flow pattern and heat transfer characteristics were observed by varying the vibration frequency and intensity. Gershuni *et al.* [6] studied the thermal convection in a rectangular enclosure which is induced by high frequency vibration under a weightlessness condition by solving the time-averaged governing equations; the flow pattern and heat transfer rates were presented in the results. Yurkov [7, 8] investigated the effects of finite frequency vibration on the square enclosure by solving the Boussinesq-approximated governing equations, and found the parametric resonant phenomenon of the Nusselt number. Biringen and Danabasoglu [9] studied the effects of gravity modulation in a thermally driven rectangular enclosure in terrestrial and microgravity environments on heat transfer phenomena; the results showed that the destabilizing and stabilizing effects of the gravity modulation agreed with the theories. Recently, Fu and Shieh [10] studied numerically the effect of the vibration frequency on the heat transfer mechanism in a square enclosure. The dimensionless frequency varied from 0 to 10^4; five characteristic flow regimes were derived in this range and a preliminary estimation was proposed to predict the resonant vibration frequency.

The papers mentioned above are related to the 'steady state' of the problem; transient processes caused by the sudden change of the environment such

NOMENCLATURE

b	vibration amplitude [m]
C_p	specific heat [J kg^{-1} K^{-1}]
g_0	standard gravitational acceleration (= 9.8 m s^{-2})
G	vibration Grashof number, $(\beta b\Omega(T_h - T_c)L)^2/2\nu^2$
k	thermal conductivity [W m^{-1} K^{-1}]
L	length of the enclosure [m]
Nu	Nusselt number
Nu_X	total Nusselt number
p	pressure [Pa]
p^*	motion pressure [Pa]
P	dimensionless pressure
Pr	Prandtl number, ν/α
Ra	Rayleigh number, $g_0\beta(T_h - T_c)L^3/(\alpha\nu)$
t	time [s]
T	temperature [K]
u, v	velocities in x and y directions [m s^{-1}]
U, V	dimensionless velocities in the x and y directions
x, y	coordinates
X, Y	dimensionless coordinates.

Greek symbols

α	thermal diffusivity [m^2 s^{-1}]
β	thermal expansion coefficient [K^{-1}]
θ	dimensionless temperature
μ	viscosity [kg m^{-1} s^{-1}]
ν	kinematic viscosity [m^2 s^{-1}]
ρ	density [kg m^{-3}]
τ	dimensionless time
$\Delta\tau$	dimensionless time increment
Ψ	dimensionless stream function
$\Psi_{\max(\text{or}\min)}$	maximum (or minimum) value of Ψ at a given instant state
ω	dimensionless frequency of vibration, $\Omega L^2/\alpha$
Ω	angular frequency of vibration [rad s^{-1}].

Subscripts

c	cold wall
h	hot wall.

Superscripts

m	iteration number.

as the wall temperature are not considered. However, the transient process is important in engineering applications like the start-up or shut-down of a process. Ivanova [11] investigated experimentally the vibration effect on the cooling process of the fluid layer between concentric cylinders and the results showed that increasing the vibration frequency or the vibration amplitude decreased the cooling time of the fluid. Duval and Jacqmin [12] studied numerically the interfacial dynamics of two miscible liquids under an oscillating gravitational field. The results showed that the interface region acted as a vortex source sheet which served as a stirring mechanism to promote local mixing. As the Stokes–Reynolds number exceeded a critical value, a chaotic structure was observed. The thermal convection in an enclosure, which is found in many industrial devices, suddenly induced simultaneously by gravity and vibration has not yet been investigated numerically.

This paper aims to solve the vibration effects on the transient thermal convection in a square enclosure caused by abrupt change of the wall temperature and vibration conditions. Based upon the results of ref. [10], the phenomena for a Rayleigh number of 10^4 influenced by the vibration frequency are more remarkable than those for a Rayleigh number of 10^6; the case for a Rayleigh number of 10^4 is then preliminarily studied and the vibrational Grashof num-

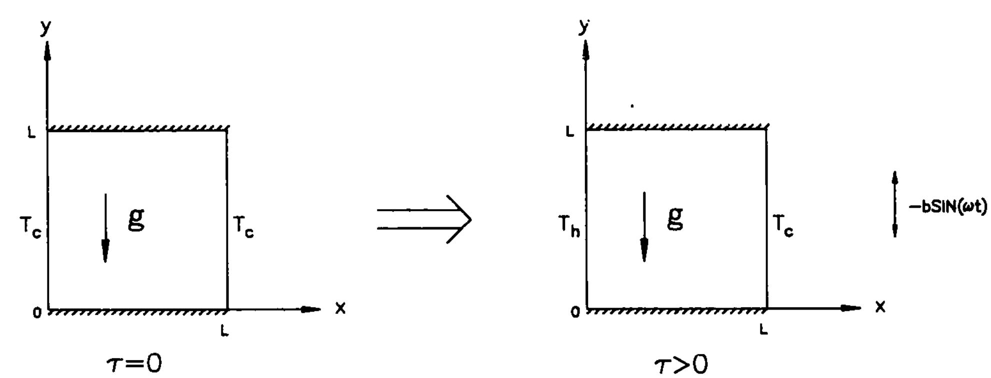

FIG. 1. Physical model.

ber is fixed at 10^6. The vibration frequencies $\omega = 100$, 900, 1100 and 5000, which are respectively located in the vibration convection regime, resonant vibration convection regime, intermediate convection regime and high frequency vibration convection regime obtained from ref. [10], are selected. The time history of the Nusselt number, stream function and the volumetric-averaged energy of the fluid are also presented.

PHYSICAL MODEL

The physical model sketched in Fig. 1 is an air-filled ($Pr = 0.71$) square enclosure with two horizontal adiabatic walls and two vertical constant temperature walls. Initially ($t = 0$), the fluid in the enclosure is stationary and the temperature of the fluid and the vertical walls is kept at T_c. Afterwards ($t > 0$), the enclosure is subjected to a vertical vibration with the displacement $-b\sin(\Omega t)$ parallel to the gravity direction, and the temperature of the left wall is raised to T_h. Then a non-inertial frame of reference traveling with the enclosure is used and b, Ω and t are respectively the vibration displacement amplitude, angular frequency and time.

In order to facilitate the analysis, the following assumptions are made:

(1) The fluid is Newtonian and the flow is two-dimensional laminar.

(2) The vibration velocity amplitude $b\Omega$ is not large and the flow is incompressible [13].

(3) The Boussinesq approximation is valid and the radiation effect is neglected.

The following variables are introduced:

$$\tau = t/(L^2/\alpha), \quad X = x/L, \quad Y = y/L,$$
$$U = u/(\alpha/L), \quad V = v/(\alpha/L),$$
$$\theta = (T-T_c)/(T_h-T_c), \quad P = p^*/(\rho_c\alpha^2/L^2),$$
$$\omega = \Omega L^2/\alpha, \quad Pr = \nu/\alpha, \tag{1}$$
$$Ra = g_0\beta(T_h-T_c)L^3/(\alpha\nu);$$
$$G = (\beta b\Omega(T_h-T_c)L)^2/2\nu^2.$$

With these assumptions and the introduction of the above dimensionless variables, the dimensionless

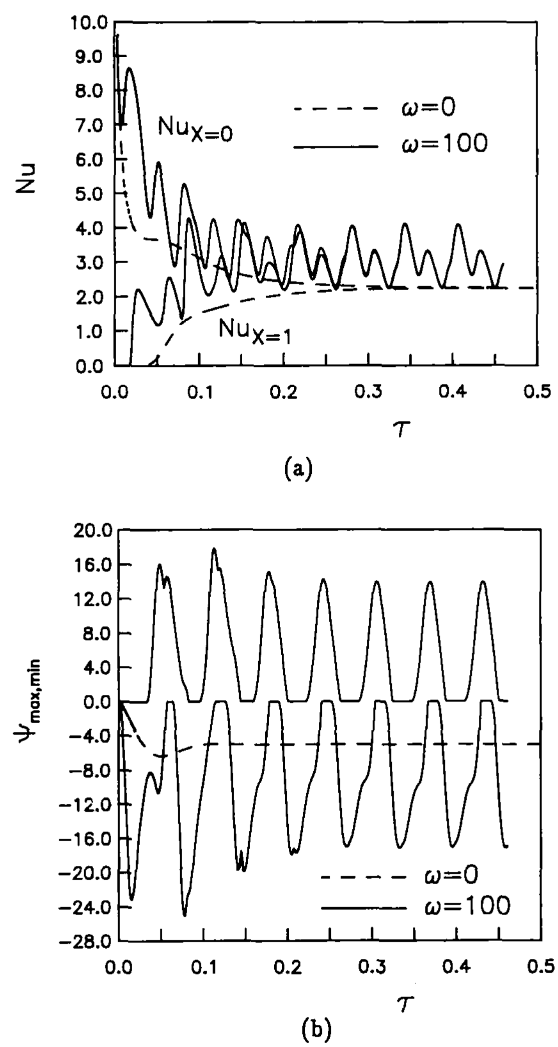

FIG. 2. Variations of the total Nusselt numbers along vertical walls and the maximum and minimum stream functions for $\omega = 100$: (a) Nusselt numbers; (b) stream functions.

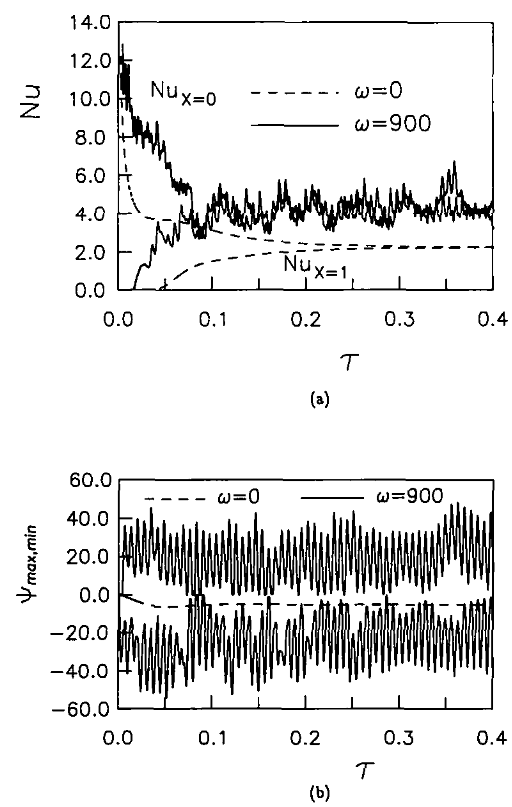

FIG. 3. Variations of the total Nusselt numbers along vertical walls and the maximum and minimum stream functions for $\omega = 900$: (a) Nusselt numbers; (b) stream functions.

governing equations can be expressed as follows:

$$\frac{\partial U}{\partial X}+\frac{\partial V}{\partial Y}=0 \quad (2)$$

$$\frac{\partial U}{\partial \tau}+U\frac{\partial U}{\partial X}+V\frac{\partial U}{\partial Y}=-\frac{\partial P}{\partial X}+Pr\left(\frac{\partial^2 U}{\partial X^2}+\frac{\partial^2 U}{\partial Y^2}\right) \quad (3)$$

$$\frac{\partial V}{\partial \tau}+U\frac{\partial V}{\partial X}+V\frac{\partial V}{\partial Y}=-\frac{\partial P}{\partial Y}+Pr\left(\frac{\partial^2 V}{\partial X^2}+\frac{\partial^2 V}{\partial Y^2}\right)+Pr(Ra+\omega\sqrt{(2G)}\sin\omega\tau)\theta \quad (4)$$

$$\frac{\partial \theta}{\partial \tau}+U\frac{\partial \theta}{\partial X}+V\frac{\partial \theta}{\partial Y}=\frac{\partial^2 \theta}{\partial X^2}+\frac{\partial^2 \theta}{\partial Y^2}, \quad (5)$$

in which G is the vibration Grashof number [5].

The boundary conditions are as follows:

$\tau=0$

$$U=V=\theta=0$$

$\tau>0$

$$X=0,\quad U=V=0,\quad \theta=1$$

$$X=1,\quad U=V=\theta=0$$

$$Y=0 \text{ and } Y=1,\quad U=V=\partial\theta/\partial Y=0. \quad (6)$$

SOLUTION METHOD

The penalty Galerkin finite element method with a Newton–Raphson algorithm and a backward difference scheme dealing with the time term, which is similar to the one used in Fu *et al.* [14], are employed to solve the governing equations (2)–(5). Nine-node quadratic isoparametric elements are used to express the velocities and temperature terms, which are integrated by 3×3 Gaussian quadrature, while the pressure term is expressed by the penalty function and integrated by 2×2 Gaussian quadrature. To determine a suitable grid size, the solution of the static case $Ra=10^6$, $\omega=0$ is computed for various meshes to compare with the benchmark solution of de Vahl Davis [15]. A final grid size of 15×15 elements was chosen for this study; the maximum error is 1.85% for $Nu_{X=0}$, while the errors of the other terms are smaller than 1%. The time increments are selected as follows by numerical experiments:

$$0<\tau\leqslant 0.02 \quad \Delta\tau=10^{-5}$$

$$0.02<\tau \quad \Delta\tau^{m+1}=\min(\Delta\tau^m\times1.02,\ T/NCYCLE)$$

where T is the period of the vibration, $NCYCLE$ is the number of time increments used in a vibration

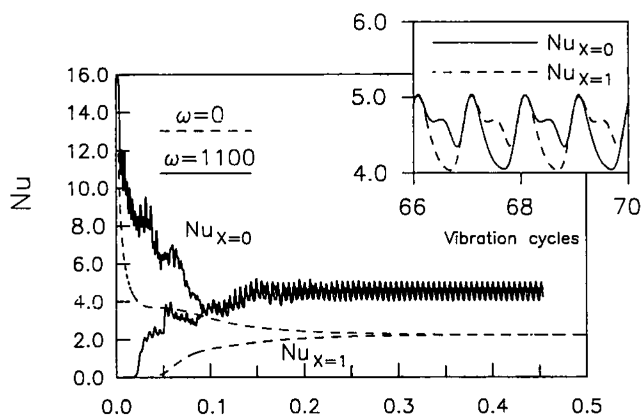

(a)

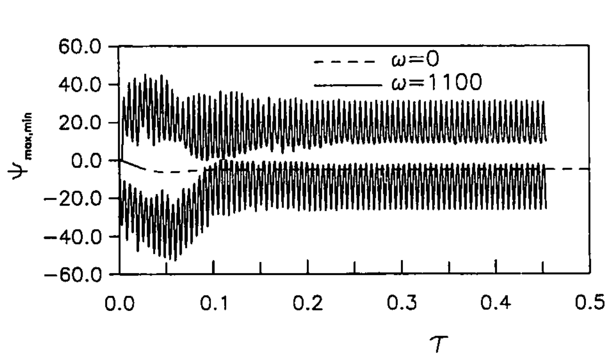

(b)

FIG. 4. Variations of the total Nusselt numbers along vertical walls and the maximum and minimum stream functions for $\omega=1100$: (a) Nusselt numbers; (b) stream functions.

cycle, $NCYCLE = 128$ for $\omega = 100, 1100, 5000$ and $NCYCLE = 256$ for $\omega = 900$.

In order to validate the accuracy of this method, the global energy balance error Err is used to examine the errors resulting from the method. Err is defined by the following equation:

$$Err = \left| \frac{Q_L - Q_R - Q_E}{Q_L} \right| \tag{7}$$

where

$$Q_L \left(= \int_0^L -k \frac{\partial T}{\partial x}\bigg|_{x=0} \mathrm{d}y \right)$$

is the amount of heat transferred in from the left wall,

$$Q_R \left(= \int_0^L -k \frac{\partial T}{\partial x}\bigg|_{x=L} \mathrm{d}y \right)$$

is the amount of heat transferred out from the right wall, and

$$Q_E \left(= \int_0^L \int_0^L \rho C_p \frac{\partial T}{\partial t} \mathrm{d}x\,\mathrm{d}y \right)$$

is the increasing rate of the internal energy of the fluid.

During the computation, Err is less than 1% for $\omega = 100$ and less than 2% for $\omega = 1100$, and less than 2.5% for $\omega = 900$ and 5000.

The total Nusselt number Nu_X on the vertical walls is defined as

$$Nu_{X=0,1} = \int_0^1 -\frac{\partial \theta}{\partial X}\bigg|_{X=0,1} \mathrm{d}Y. \tag{8}$$

The dimensionless stream function Ψ is obtained by integrating $U = \partial\Psi/\partial Y$ with $\Psi = 0$ along the walls.

RESULTS AND DISCUSSION

In Figs. 2–5, the time history of the variations of the total Nusselt numbers $Nu_{X=0,1}$ on the vertical walls and the maximum and minimum of the stream functions $\Psi_{max,min}$ are presented for $\omega = 100$, 900, 1100 and 5000. The dashed lines in the figures represent the static case ($Ra = 10^4$, $\omega = 0$). In general, $Nu_{X=0}$ decreases from infinity and $Nu_{X=1}$ increases from zero to a periodic value at steady state. Ψ_{max} represents the maximum stream function of the flow which rotates counter-clockwise and Ψ_{min} represents the minimum

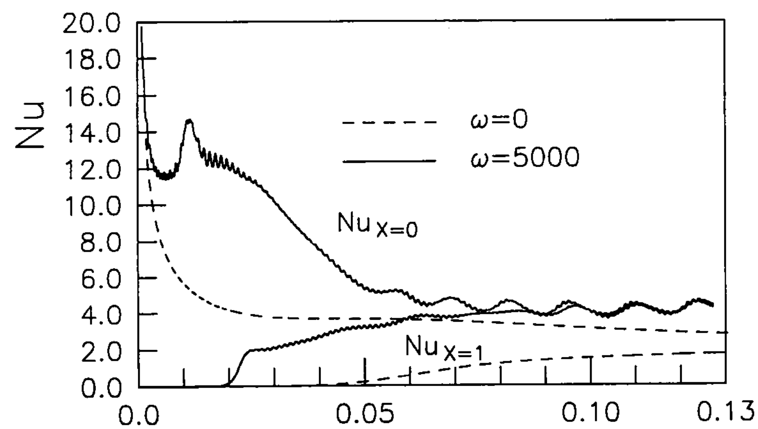

(a)

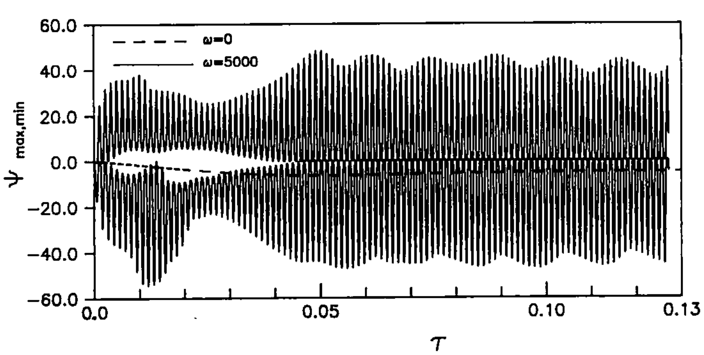

(b)

FIG. 5. Variations of the total Nusselt numbers along vertical walls and the maximum and minimum stream functions for $\omega = 5000$: (a) Nusselt numbers; (b) stream functions.

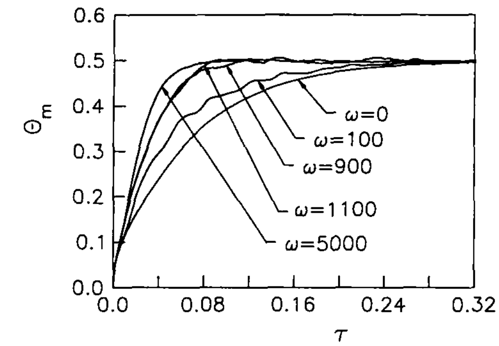

FIG. 6. Variation of the bulk-mean temperature θ_m.

stream function of the flow which rotates clockwise in the enclosure at an instant.

Figures 2(a) and (b) are the variations of $Nu_{X=0,1}$ and $\Psi_{max,min}$ with respect to time for $\omega = 100$. During the transient process, both the total Nusselt numbers for the vibrational case are still larger than those for the static case, and at the steady state the minimum total Nusselt numbers $Nu_{X=0}$ and $Nu_{X=1}$ for the vibrational case are almost equivalent to that for the static case, which indicates that the vibration frequency enhances the heat transfer rate for the $\omega = 100$ case. The transient times, from the beginning to the steady state, are almost equivalent for the static ($\omega = 0$) and

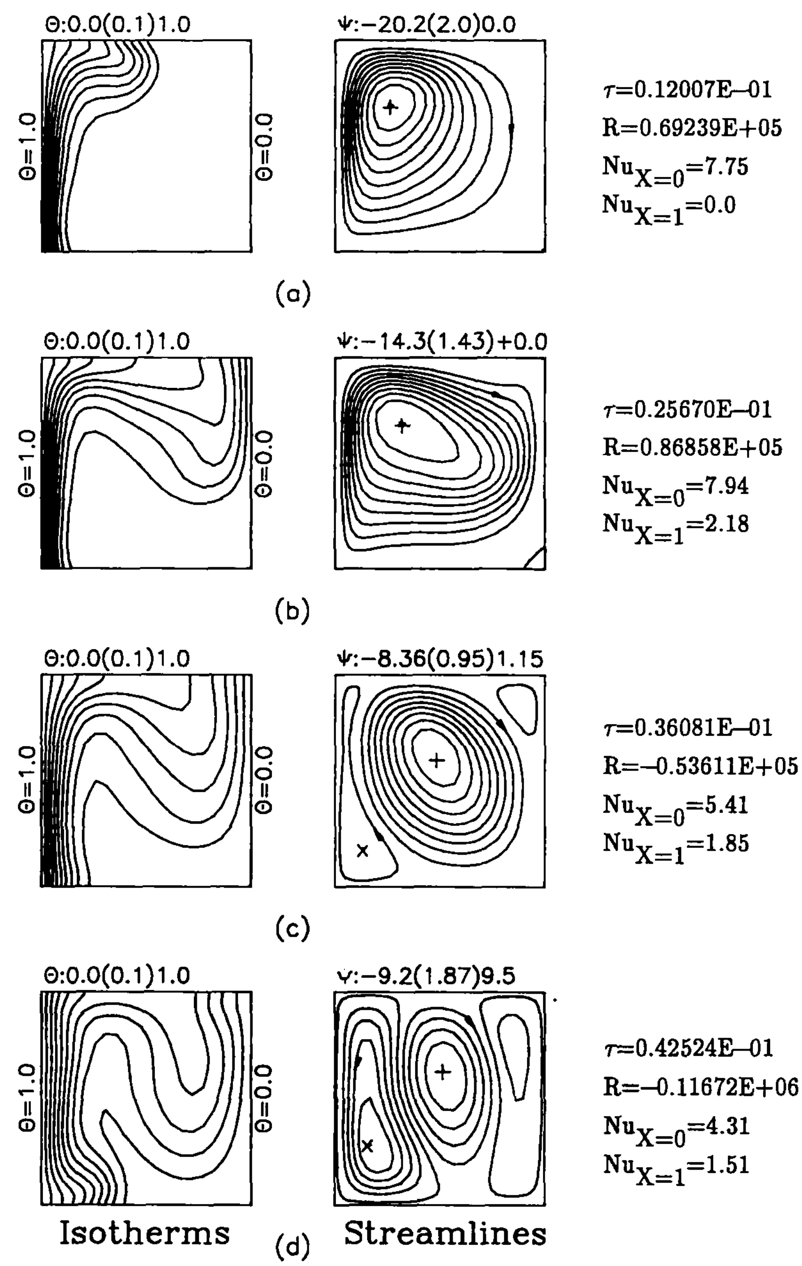

FIG. 7. Isotherms and streamlines for $\omega = 100$.

vibrational ($\omega = 100$) cases. In Fig. 2(b), Ψ_{min} and Ψ_{max} appear alternately and are stronger than those of the static case, which causes the heat transfer rate of the vibrational case to be greater than that of the static one ($\omega = 0$), shown in Fig. 2(a).

In Figs. 3(a) and (b), the variations of $Nu_{X=0,1}$ and $\Psi_{max,min}$ with respect to time for $\omega = 900$ are shown. In Fig. 3(a), both the variations of the Nusselt numbers and flow intensities of the vibrational case not only vary irregularly but also are not equivalent during the whole process, which means that the heat transferred in from the left wall is not equal to the heat transferred out from the right wall. The variational range and tendency of both intensities of Ψ_{max} and Ψ_{min} are similar. This phenomenon is different from that shown in ref. [10], which has only a dominant flow intensity and a periodic solution at steady state. The reason suggested is that the steady state solution for $\omega = 900$ in ref. [10] is obtained from calculating the lower adjoining frequency solution at the steady state; in turn, the initial condition used in ref. [10] is different from that used in this study. The difference between the total Nusselt numbers of the left and right walls will cause the internal energy of the fluid to vary continuously.

The variations of $Nu_{X=0,1}$ and $\Psi_{max,min}$ with respect

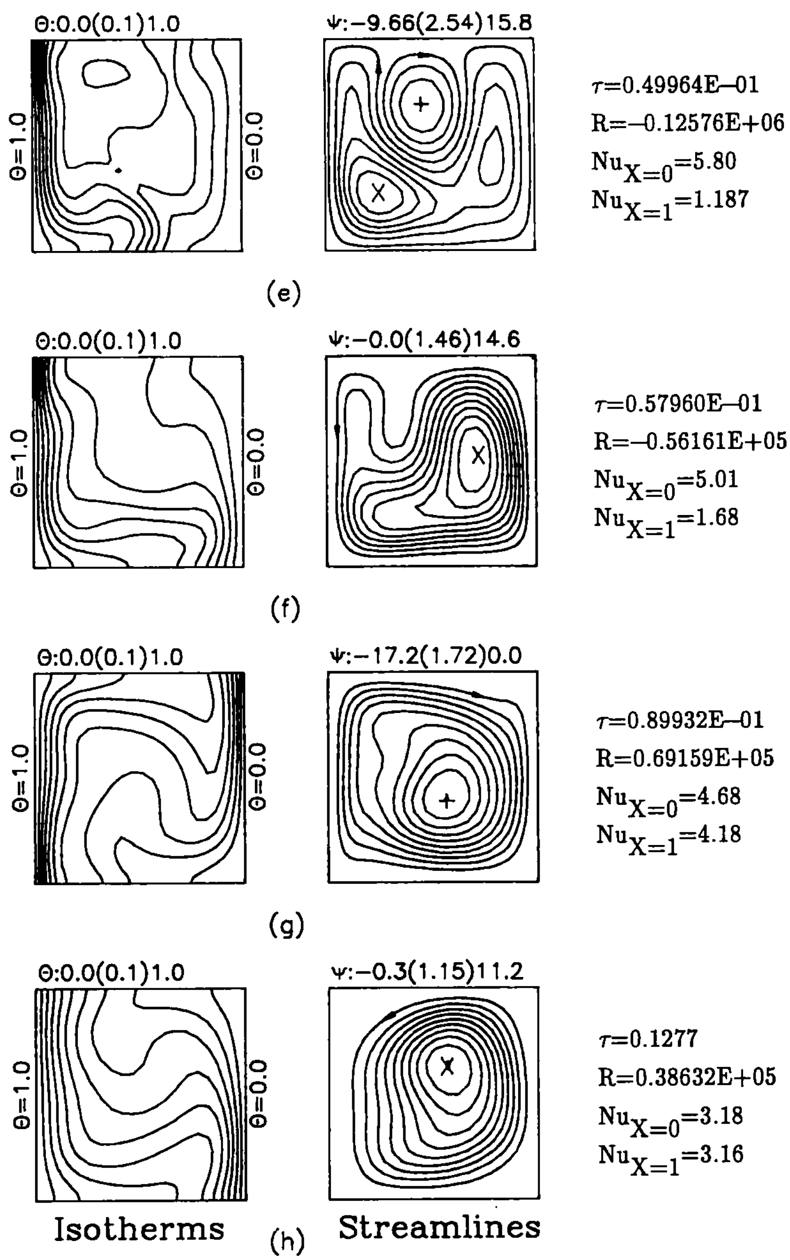

FIG. 7—*Continued.*

to time for $\omega = 1100$ are shown in Figs. 4(a) and (b). The Nusselt numbers shown in Fig. 4(a) are also irregular in the transient process before $\tau = 0.1$ and a minute undershoot ($\tau = 0.1$) of the Nusselt number occurs. The heat transfer rate in the steady state is about twice that of the static case. The Nusselt numbers of the left and right walls in the periodic steady state have a 2π phase shift, as shown in the inset of Fig. 4(a). The phenomenon of the out-of-phase left and right wall Nusselt numbers is caused by the unsymmetrical flow structure, as shown in Fig. 10. The flow intensities of Ψ_{max} and Ψ_{min} shown in Fig. 4(b) have an overshoot near $\tau = 0.06$, and at steady state the intensities of Ψ_{min} and Ψ_{max} vary alternately, but the magnitude of Ψ_{max} is greater than that of Ψ_{min}. Opposite to $\omega = 900$, at the steady state an irregular steady state solution is obtained in ref. [10], but a periodic solution is obtained in this study. As the vibration frequency is increased gradually and passes through the resonant frequency, which approximately equals 1000 estimated by ref. [10], the driving force R cannot maintain the strong resonant flow and the flow collapses into an irregular motion, which causes the solutions to be irregular in ref. [10]. On the contrary, in the transient process, the flow is excited from a stationary condition, no resonant flow occurs in the

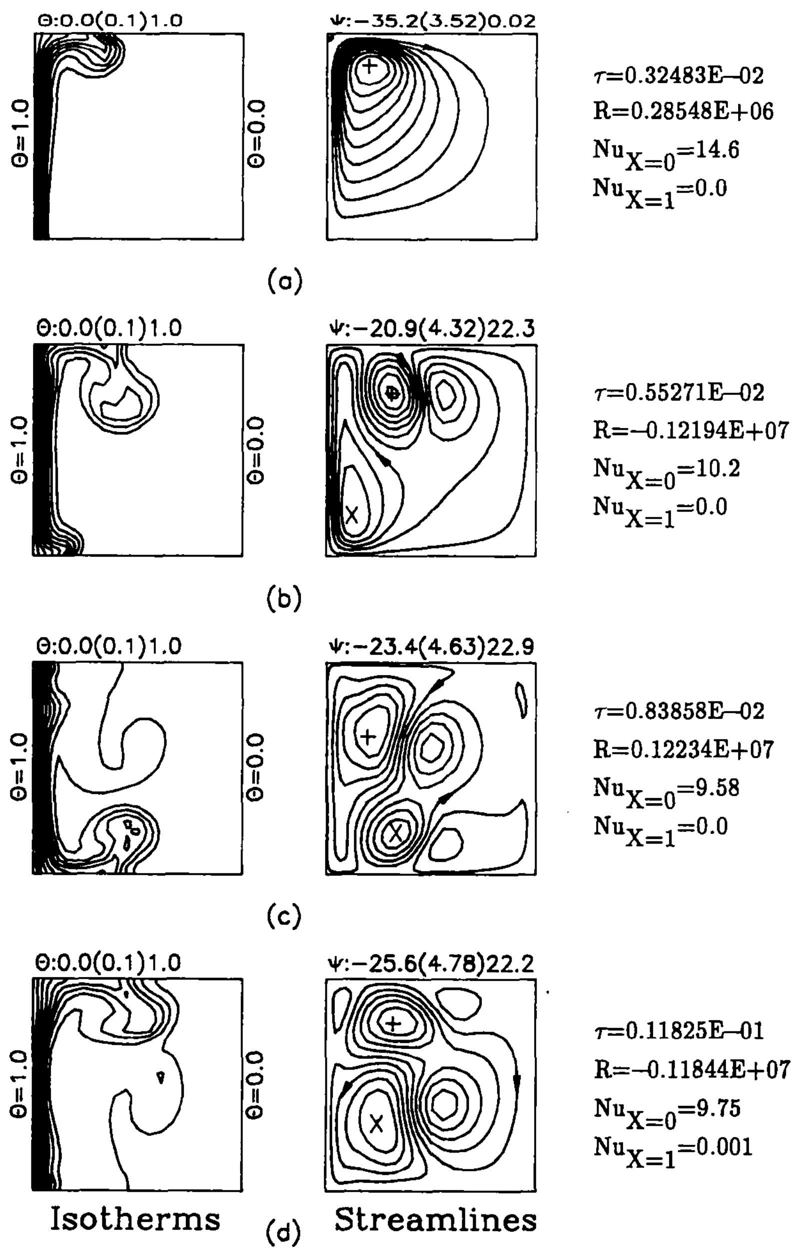

FIG. 8. Isotherms and streamlines for $\omega = 900$.

process and the flow finally approaches a periodic motion in this study.

Figures 5(a) and (b) show the variations of $Nu_{X=0,1}$ and $\Psi_{max,min}$ with respect to time for $\omega = 5000$. Because the vibration period is smaller than the time scale of the thermal boundary layer, the oscillation of the Nusselt number within one vibration cycle becomes very small. It is seen from Fig. 5(b) that the oscillating flow is constructed before $\tau = 0.01$ (Ψ_{max}, $|\Psi_{min}| > 0$). At time $\tau \cong 0.011$, the fact that $Nu_{X=0}$ overshoots together with the increase of intensity of the clockwise-rotating flow (Ψ_{min}) is significant, and is caused by the instability of the thermal boundary layer near the hot wall. The neck of the flow intensity near $\tau = 0.03$ in Fig. 5(b) is caused by the beginning of stratification of the core region. At steady state ($\tau > 0.1$), a second frequency is about 11 times the vibration period. The heat transfer rate and flow intensity are much higher than those of the static case, and the transient time is much shorter than that in the static case.

Figure 6 indicates the variations of the bulk mean temperature θ_m, which is defined as

$$\theta_m = \int_0^1 \int_0^1 \theta \, dX \, dY. \tag{9}$$

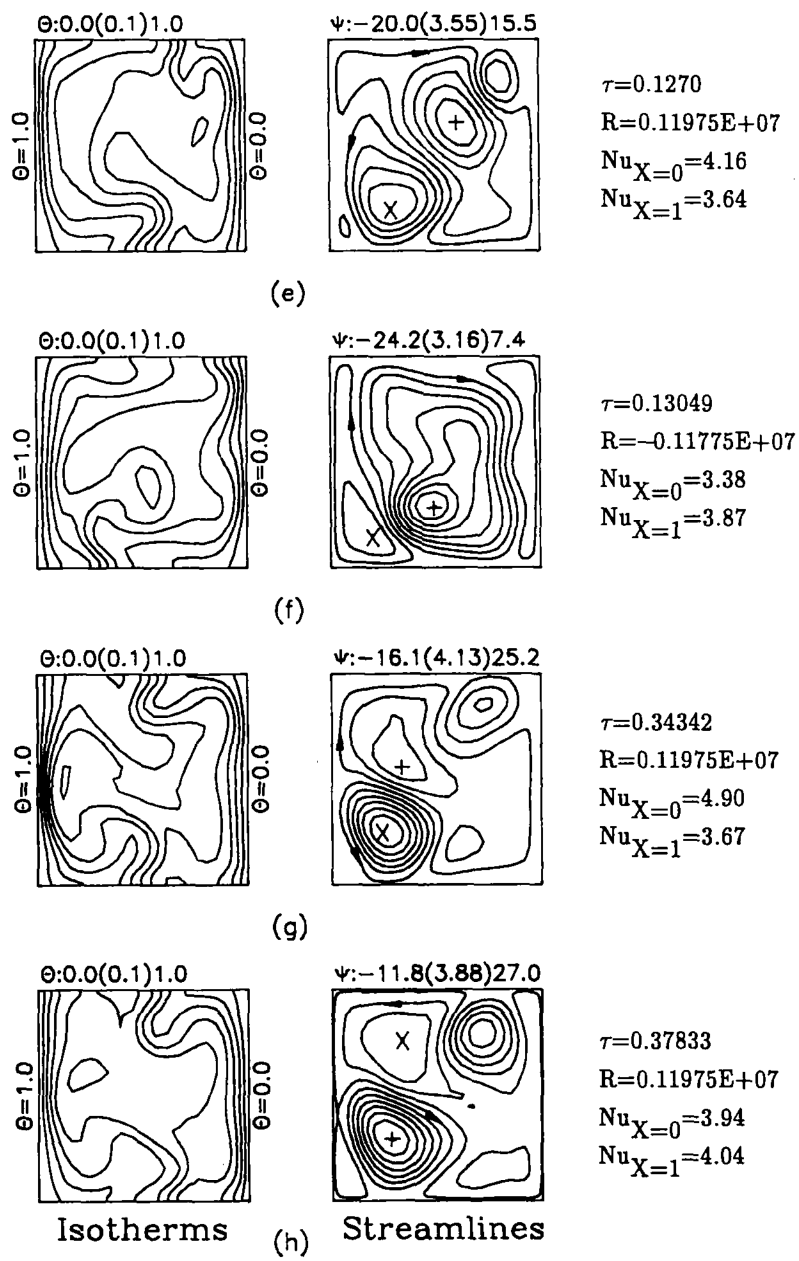

FIG. 8—*Continued.*

The time when the bulk mean temperature θ_m reaches 0.5 represents the heating effectiveness of this process. From the figure, the higher the vibration frequency, the more effective the heating process. For $\omega = 900$, even after a long time, the bulk mean temperature θ_m still fluctuates about 0.5 due to the irregular variations of the total Nusselt numbers of the left and right walls. For $\omega = 1100$, the bulk mean temperature θ_m varies periodically at steady state with a small amplitude about 0.5 due to the phase lag between the total Nusselt numbers of the left and right walls.

The variations of isotherms and streamlines during the transient process are shown in Figs. 7–11. The numbers above the figures represent the minimum, increment and maximum values of θ and Ψ, respectively. The stream function on the wall is zero, the sign '×' denotes the location of the maximum stream function Ψ_{max} and the sign '+' denotes the location of the minimum stream function Ψ_{min}. The symbol R represents the driving force term $(Ra+\omega\sqrt{(2G)}\sin\omega\tau)$.

Figure 7 illustrates the variations of the isotherms and streamlines for $\omega = 100$. The hot fluid intrudes into the cold wall, which causes the total Nusselt number $Nu_{X=1}$ to be larger than zero and forms a

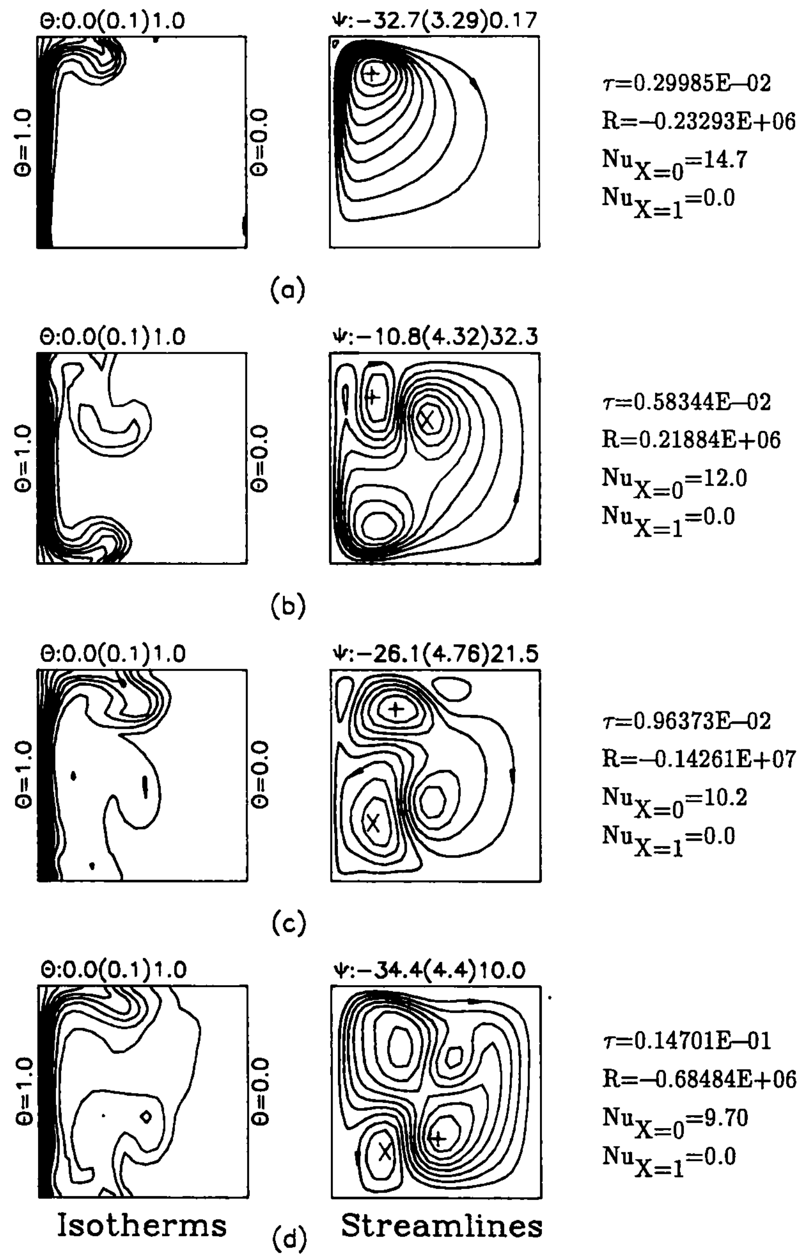

FIG. 9. Isotherms and streamlines for $\omega = 1100$.

rotating cell in a vibration cycle ($T = 0.06283$). The driving force R varies from positive to negative values alternately, which causes the rotating direction of the main cell to change. The clockwise rotating cell changes to a counter-clockwise rotating cell, which is illustrated in Figs. 7(b)–(f), and the fully developed clockwise and counter-clockwise rotating flows are shown respectively in Figs. 7(g) and (h).

Figure 8 illustrates the variations of the isotherms and streamlines for $\omega = 900$. The vibration period ($T = 0.00698$) is shorter than the time of the hot fluid moving from the hot wall to the cold wall. The 'warm front' of the fluid (the $\theta = 0.1$ isotherm) moves from the hot wall to the cold wall by the development of mushroom-like isotherms, which differs from the phenomenon of the core region stratified gradually in the $\omega = 100$ case. The vortices shed from the upper and lower corners of the hot wall alternately, as shown in Figs. 8(a)–(d). In Fig. 8(a), a clockwise rotating cell is formed in the left upper corner with the hot fluid intruding into the core region, but the driving force R is reversed before the hot fluid reaches the cold wall in Fig. 8(b). Consequently, a new counter-clockwise rotating cell develops near the left lower corner and the original clockwise rotating cell atrophies gradually. As shown in Figs. 8(e)–(h), even after

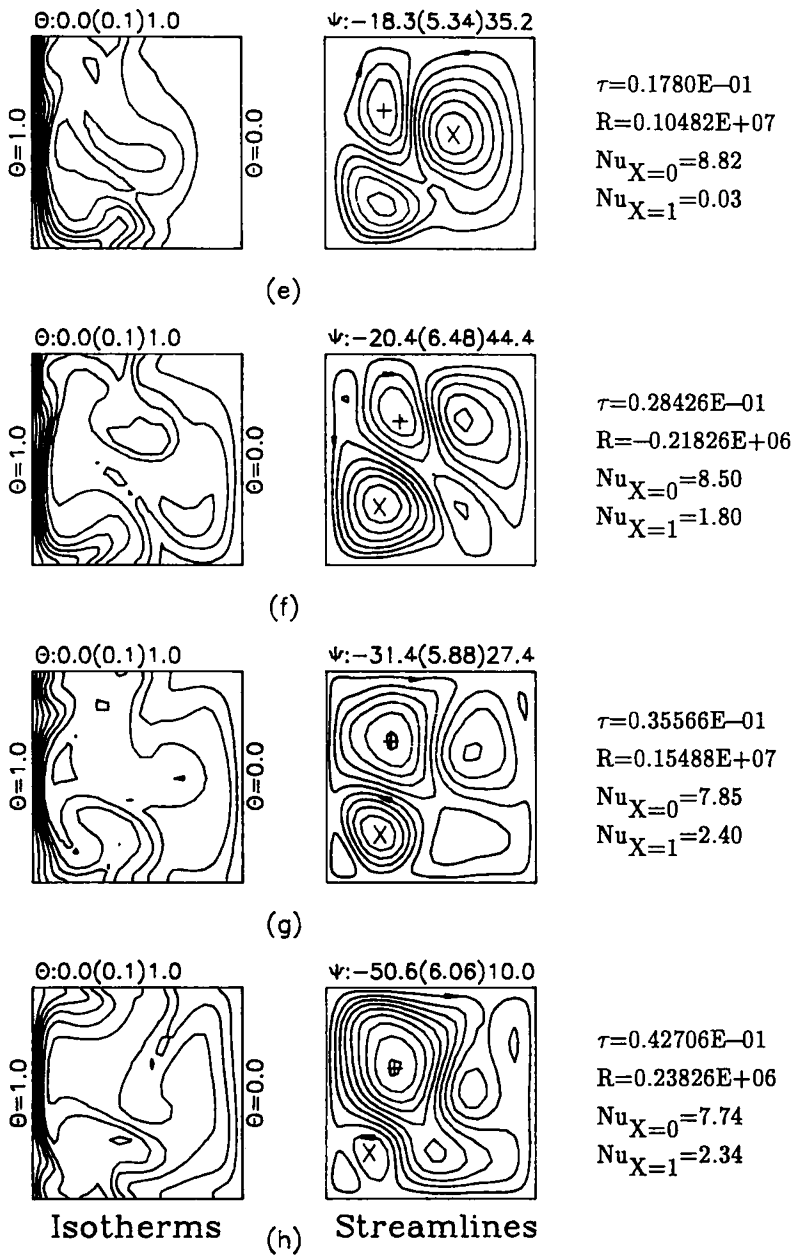

FIG. 9—*Continued.*

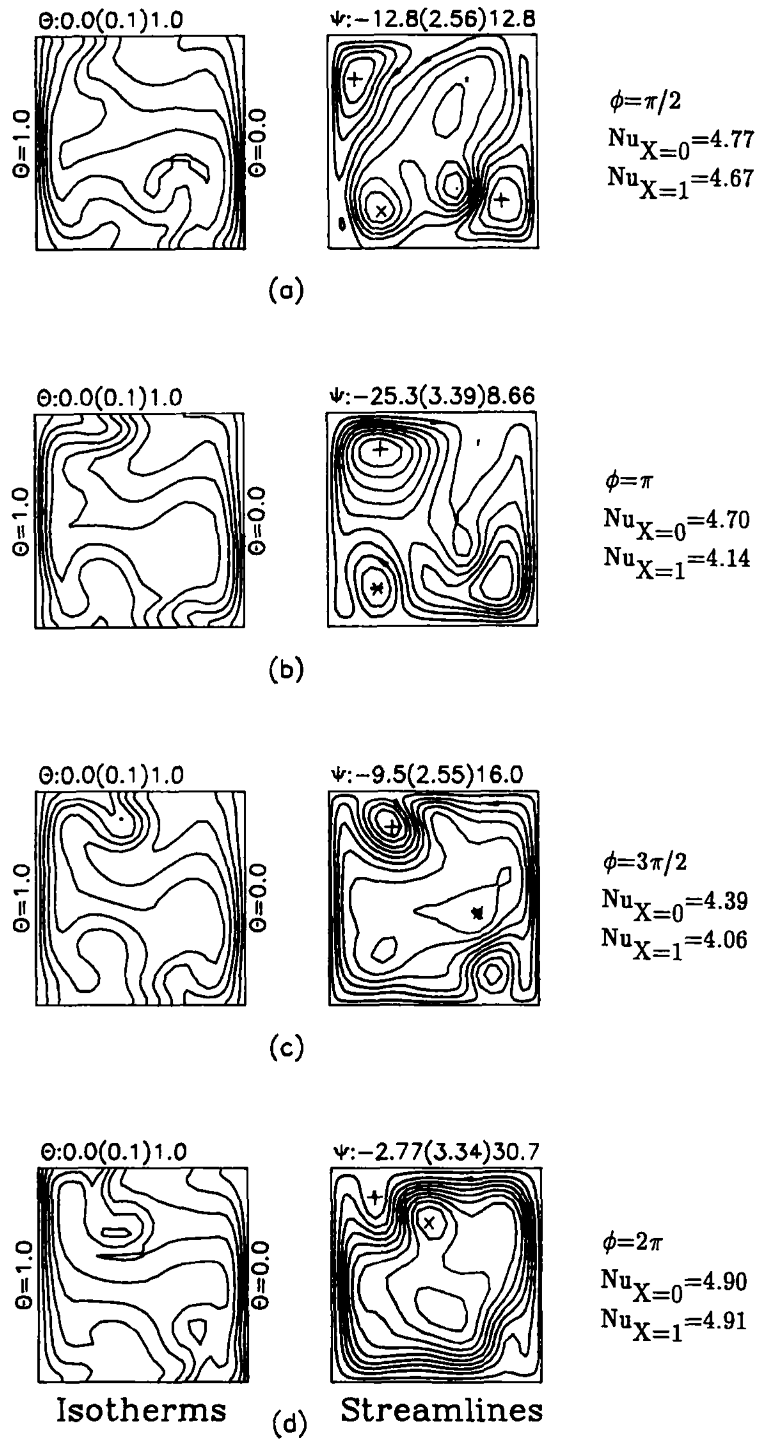

FIG. 10. Isotherms and streamlines at steady state for $\omega = 1100$.

a long time, the flows are still irregular, and the vortices shed and dissipate continuously, which causes an unsymmetrical flow and temperature structure to be formed. Furthermore, under the same vibration phase as shown in Figs. 8(g) and (h), the flow patterns cannot be consistent. Strictly speaking, the steady state does not exist in this situation. The phenomenon is different from the flow in ref. [10]. This suggests that the continuous growing and atrophying of the vortices in the upper and lower corners causes the total Nusselt numbers on the left and right walls not to be equivalent in Fig. 3(a).

The variations of isotherms and streamlines for $\omega = 1100$ during the transient process shown in Figs. 9(a) and (b) are similar to those for $\omega = 900$. The vortices shed and dissipate continuously from the

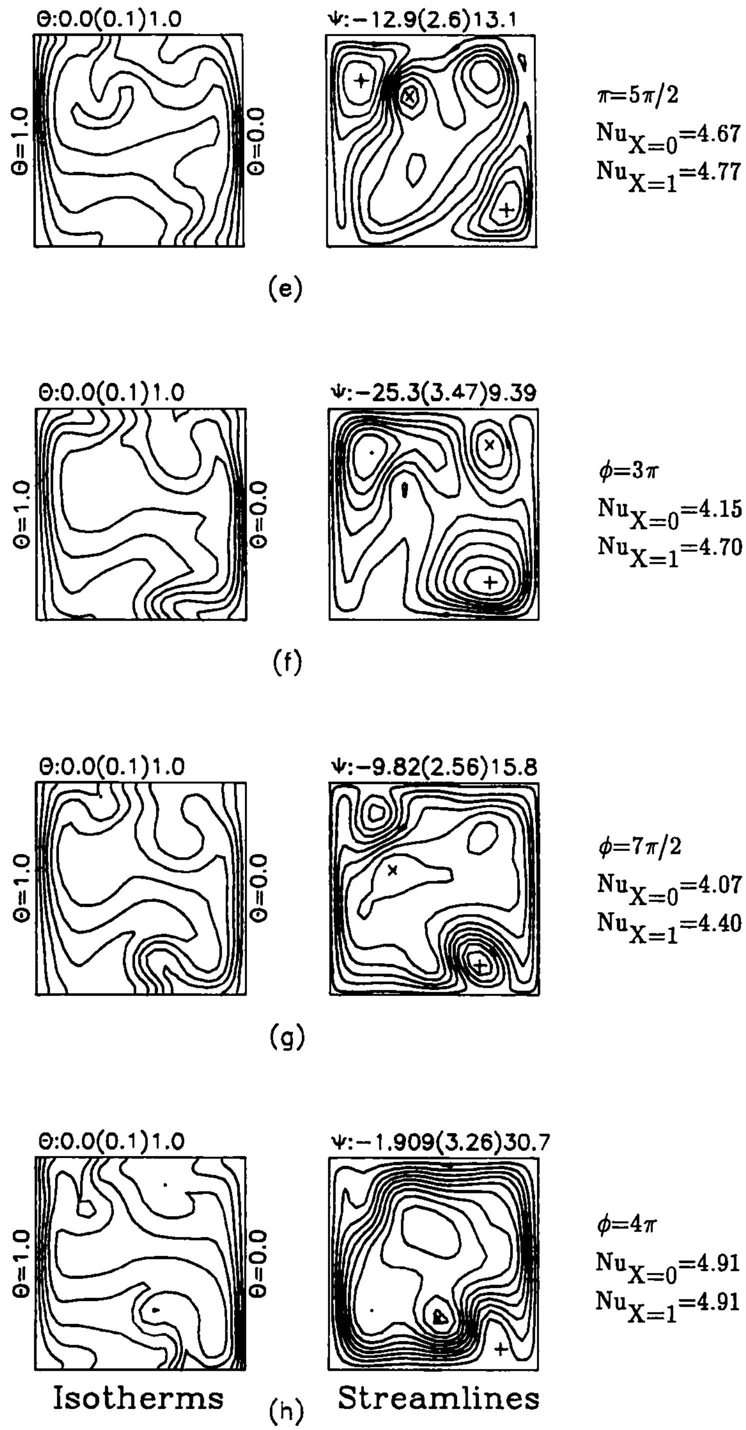

FIG. 10—*Continued.*

upper and lower corners, which causes the flow patterns to be complicated.

However, the variations of total Nusselt numbers become periodically regular after $\tau > 0.2$, shown in Fig. 4(a), and the flow period is composed of two vibration cycles. The accompanying figures, which illustrate the variations of isotherms and streamlines, are shown in Figs. 10(a)–(h), where ϕ is the phase angle. In the figures, the growing and atrophying of vortices are still observed, and the unsymmetrical flow structure seems to be the main reason for the total Nusselt numbers of the left and right walls not being consistent.

Figure 11 shows the isotherms and streamlines for $\omega = 5000$. Since the vibration frequency ω is high, the buoyancy force induced by the vibration is definitely

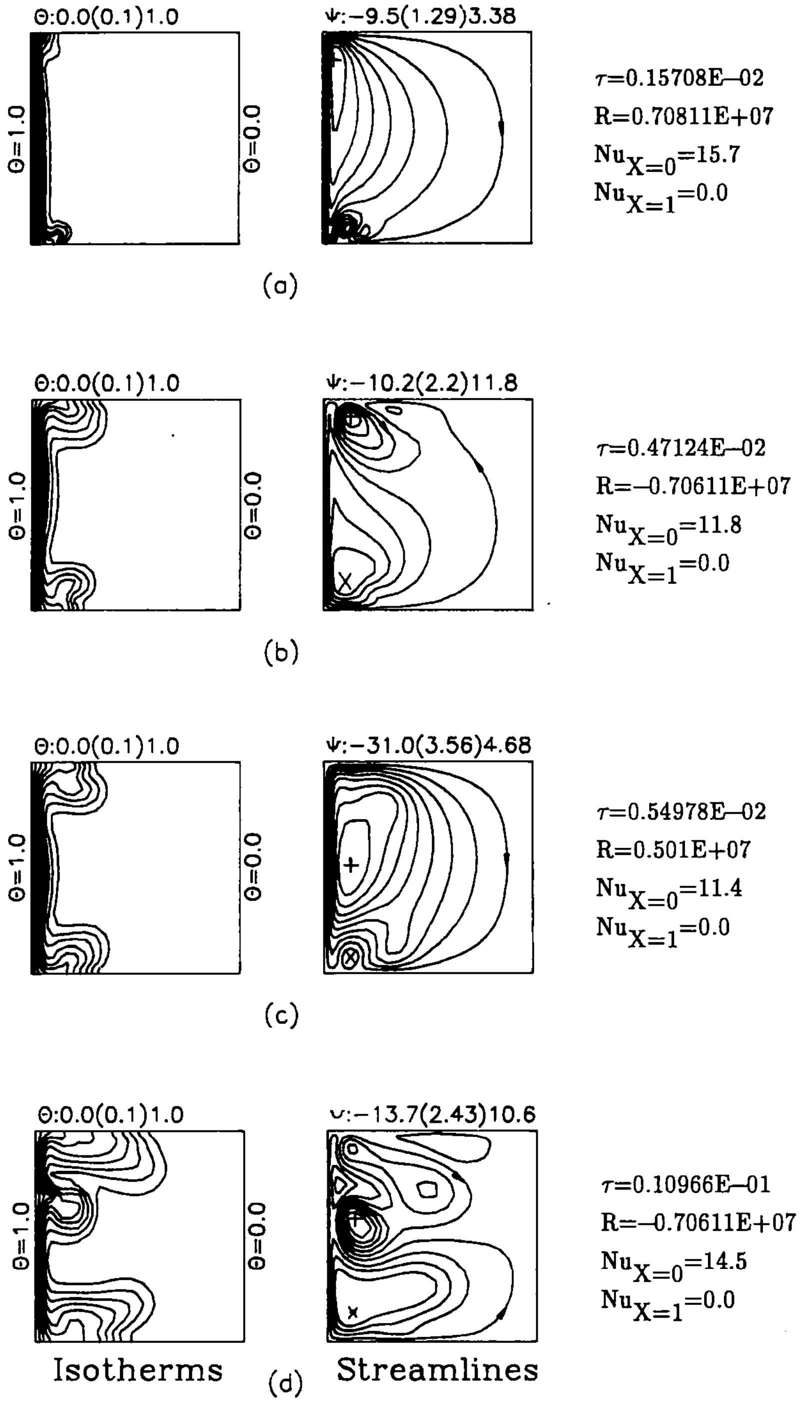

FIG. 11. Isotherms and streamlines for $\omega = 5000$.

dominant. As a result, the development of the isotherms is almost symmetric at the center line of the vertical walls initially, which is very different from that of the low frequency situation. The rotating direction of the main cell varies in synchronization with the variation of the driving force R. Later, the development of the isotherm distributions starts to be unstable, as shown in Fig. 11(d), which causes a remarkable overshoot to occur on the left wall total Nusselt number distribution curve at time $\tau \cong 0.01$, as shown in Fig. 5(a). Finally, in Fig. 11(h), the core region is stratified gradually, which weakens the flow and heat transfer rate.

CONCLUSIONS

The effects of vibration on the transient thermal convection in a square enclosure are investigated

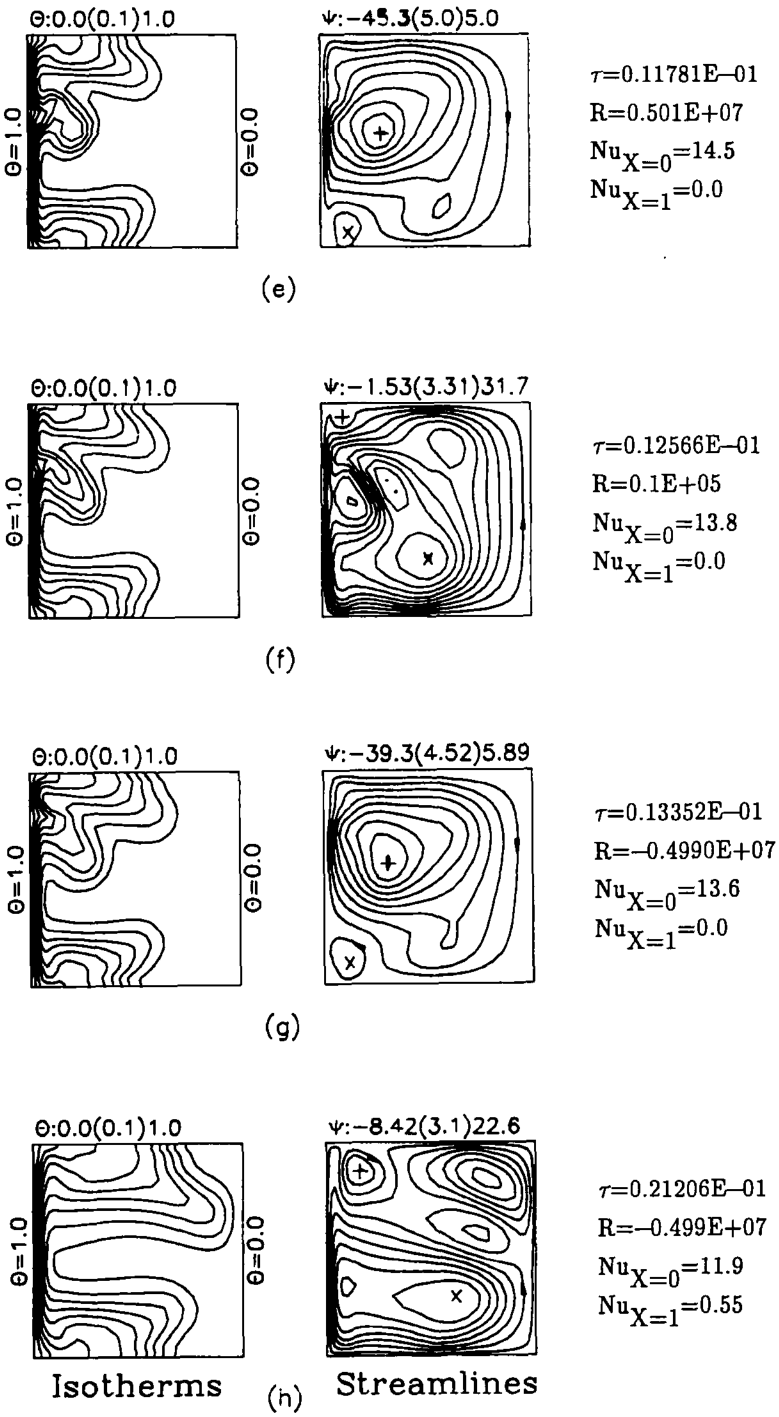

FIG. 11—*Continued.*

numerically. Four vibration frequencies ($\omega = 100$, 900, 1100, 5000) are studied with $Ra = 10^4$ and $G = 10^6$. Several conclusions can be drawn.

(1) At low frequency ($\omega = 100$), the hot fluid intrudes into the cold wall in a vibration cycle, and the flow alternates between the clockwise and counterclockwise rotating cells.

(2) At intermediate frequencies ($\omega = 900$, 1100), the hot wall becomes a vortex generator which sheds the vortices from the upper and lower corners. The growing and atrophying of vortices cause the heat transfer rate to vary irregularly and the total Nusselt numbers of the left and right walls not to be consistent.

(3) At high frequency ($\omega = 5000$), an overshoot is found on the left wall total Nusselt number distribution which is caused when the thermal boundary layer begins to be unstable.

(4) The higher the vibration frequency is, the quicker the steady state is reached.

Acknowledgement—The support of this work by the National Science Council, Taiwan, R.O.C. under contract NSC80-0401-E-009-16 is gratefully acknowledged.

REFERENCES

1. Y. Kamotani, A. Prasad and S. Ostrach, Thermal convection in an enclosure due to vibrations aboard spacecraft, *AIAA J.* **19,** 511–516 (1981).
2. M. Wadih and B. Roux, Natural convection in a long vertical cylinder under gravity modulation, *J. Fluid Mech.* **193,** 391–415 (1988).
3. P. D. Richardson, Effects of sound and vibrations on heat transfer, *AMR* **20,** 201–217 (1967).
4. R. E. Forbes, C. T. Carley and C. J. Bell, Vibration effects on convective heat transfer in enclosures, *J. Heat Transfer* 429–438 (1970).
5. A. A. Ivanova and V. G. Kozlov, Vibrationally gravitational convection in a horizontal cylindrical layer, *Heat Transfer—Sov. Res.* **20,** 235–247 (1988).
6. G. Z. Gershuni, E. M. Zhukhovitskii and Yu S. Yurkov, Vibrational thermal convection in a rectangular cavity, *Izv. AN SSSR, Mech. Zhidk. Gaza* No. 4, 94–99 (1982).
7. Yu. S. Yurkov, Vibration-induced thermal convection in a square cavity in weightlessness at arbitrary frequencies. In *II Vsesoyuznyye seminor po gidromekhanike i teplomassoobmenu V nevesomosti* [Tezisy dokladov], pp. 36–37 (1981).
8. Yu. S. Yurkov, Vibration-induced thermal convection in a square cavity in weightlessness (finite frequencies). In *Konvektivnyye techeniya*, pp. 98–103. Convective Perm Teachers' Institute, Perm (1981).
9. S. Biringen and G. Danabasoglu, Computation of convective flow with gravity modulation in rectangular cavities, *J. Thermophys.* **4,** 357–365 (1990).
10. W. S. Fu and W. J. Shieh, The study of thermal convection in an enclosure induced simultaneously by gravity and vibration, *Int. J. Heat Mass Transfer* **35,** 1695–1710 (1992).
11. A. A. Ivanova, Influence of vibrations of the unsteady-state convective heat transfer in a cylindrical cavity, *Heat Transfer—Sov. Res.* **20,** 248–251 (1988).
12. W. M. B. Duval and D. A. Jacqmin, Interfacial dynamics of two liquids under an oscillating gravitational field, *AIAA J.* **28,** 1933–1941 (1990).
13. R. J. Schoenhals and J. A. Clark, Laminar free convection boundary-layer perturbations due to transverse wall vibration, *J. Heat Transfer* 225–234 (1962).
14. W. S. Fu, J. C. Perng and W. J. Shieh, Transient laminar natural convection in an enclosure partitioned by an adiabatic baffle, *Numer. Heat Transfer* **16A,** 325–359 (1989).
15. G. de Vahl Davis, Natural convection of air in a square cavity: a bench mark numerical solution, *Int. J. Numer. Meth. Fluids* **3,** 249–264 (1983).